Zeitschrift: Eclogae Geologicae Helvetiae

Band: 94 (2001)

Heft: 3

Artikel: Integration of geophysical methods to study the fold geometry of the Tschera nappe, eastern Switzerland

Autor: Gurk, Marcus / Bosch, Frank / Challandes, Nathalie

DOI: https://doi.org/10.5169/seals-168898

0012-9402/01/030329-10 $1.50 + 0.20/0
Birkhäuser Verlag, Basel, 2001

Eclogae geol. Helv. 94 (2001) 329–338

Integration of geophysical methods to study the fold geometry of the Tschera nappe, eastern Switzerland

MARCUS GURK[1], FRANK BOSCH[2], NATHALIE CHALLANDES[3] & JÜRGEN BIGALKE[4]

Keywords: Self-potential, magnetic method, VLF, RF-EM, induction arrows, graphite

ABSTRACT

A combined survey using the self-potential (SP), magnetic profiling and continuously measuring Radio Frequency-Electromagnetic (RF-EM) method has been carried out to study the fold geometry and the lithostratigraphy of the Tschera nappe. The Schams nappe sub-unit is located between the steep structural contact of the Mesozoic sediments (Bündnerschiefer) and the crystalline Penninic Suretta nappe (Rofna Porphyr) in Graubünden, eastern Switzerland.

Originally, the measurements have been initiated to give evidence for the existence or the absence of a presumed electrical high conductivity zone of large lateral extent within this major contact. If the conductivity anomaly exists, the zone can contribute to the directional dualism of the real parts of induction arrows observed in the magnetotelluric (MT) and geomagnetic deep sounding (GDS) survey of Graubünden. Contrarily the absence of such a high conductive zone supports the magnetic distortion hypothesis for magnetic transfer function in Graubünden. This major contact is therefore an important key for the understanding of electromagnetic induction processes in the central Alps. The change of direction of the real induction arrows occurs over the entire period range (T= 1-300 s) between two MT/GDS sites over a 400 m distance on the Tschera/Gelbhorn nappe. This implies that a major contrast in conductivity with considerable lateral and vertical extent is present in this contact zone.

The first analysis of the order of a set of self-potential and magnetic anomalies images a tight fold. Since the symmetry of the anomalies allows for a north or a south vergent fold, the self-potential anomalies have been modelled to determine the most reliable geometry within the nappe.

The RF-EM method confirms the SP and magnetic anomalies and detects the structural contact on both sides of the sub-unit. Finally, the geophysical findings have been well documented by a geological survey, showing the presence of graphite in the Tschera nappe. However, the assumed presence of a super-regional conductivity zone with the required lateral and vertical extension cannot be confirmed.

ZUSAMMENFASSUNG

Die Geometrie und die Lithostratigraphie der ostschweizerischen Tscheradecke waren das Ziel einer kombinierten geophysikalischen Messreihe unter Verwendung von Eigenpotential (SP), magnetischen und kontinuierlichen Radio Frequenz-Elektromagnetischen (RF-EM) Verfahren. Die Tscheradecke ist eine Untereinheit der Schamser Decke und markiert in Graubünden den strukturellen Kontakt zwischen den mesozoischen Sedimenten (Bündnerschiefern) im Norden und der penninischen Kristallindecke Suretta (Rofna Porphyr) im Süden. Flächendeckende magnetotellurische (MT) Messungen und geomagnetische Tiefensondierungen (GDS) zeigen in Graubünden einen Richtungswechsel der reellen Induktionspfeile (T= 1-300 s). Dieser periodenunabhängige Richtungswechsel stellt sich zwischen zwei Messpunkten über eine Distanz von ca. 400 m auf der Tschera/Gelbhorn Decke ein, und weist somit auf eine grossräumige gutleitende Störzone innerhalb des Kontaktes hin.

Falls diese leitfähige Störzone existiert, kann sie eine Erklärung für das beobachtete Verhalten der Induktionspfeile liefern. Dementgegen deutet das Ausbleiben einer angenommenen grossräumigen elektrisch gutleitenden Zone in diesem Kontakt auf eine magnetische Verzerrung der Magnetfelddaten.

Die vorläufige Analyse einer Reihe von Eigenpotential- und magnetischen Anomalien zeigt eine steile Falte mit unbestimmtem Einfallsinn. Um einen genaueren Aufschluss über die Geometrie innerhalb der Tscheradecke zu erhalten, wurden die SP Daten modelliert. Die RF-EM-Messungen belegen die SP und magnetischen Ergebnisse und zeigen zusätzlich zu beiden Seiten den strukturellen Kontakt zwischen der Tscheradecke und den umliegenden Einheiten. Alle geophysikalischen Beobachtungen wurden durch eine anschliessende geologische Begehung des Messgebietes bestätigt, wie z.B. das Vorhandensein einer graphitisierten Störzone.

Die Existenz einer überregionalen elektrisch leitfähigen Störzone entlang des strukturellen Kontakts kann jedoch nicht bestätigt werden.

1 Introduction

Few case histories exist where simple geophysical methods can help the geologist to understand complex tectonic structural settings and changes in lithostratigraphy in the absence of sufficient outcrop data. In this paper, we present an approach using the combination of self-potential (SP) and magnetic method responses as lithostratigraphic markers. Additional Radio Frequency-Electromagnetic (RF-EM) soundings were performed to support the magnetic and SP techniques and to

[1] Marcus Gurk, Groupe de Géomagnétisme, Institut de Géologie, Université de Neuchâtel, Rue Emile-Argand 11, CH-2007 Neuchâtel, Switzerland. E-Mail: marcus.gurk@unine.ch

[2] Frank Bosch, Centre d'Hydrogéologie, Institut de Géologie, Université de Neuchâtel, Rue Emile-Argand 11, CH-2007 Neuchâtel, Switzerland. E-Mail: frank.bosch@unine.ch, corresponding author

[3] Nathalie Challandes, Institut de Géologie, Rue Emile-Argand 11, Université de Neuchâtel, CH-2007 Neuchâtel, Switzerland. E-Mail: nathalie.challandes@unine.ch

[4] Jürgen Bigalke, Institute of Meteorology and Geophysics, University of Frankfurt, Feldbergstrasse 47, D-60323 Frankfurt, am Main, Germany. E-mail: bigalke@geophysik.uni-frankfurt.de

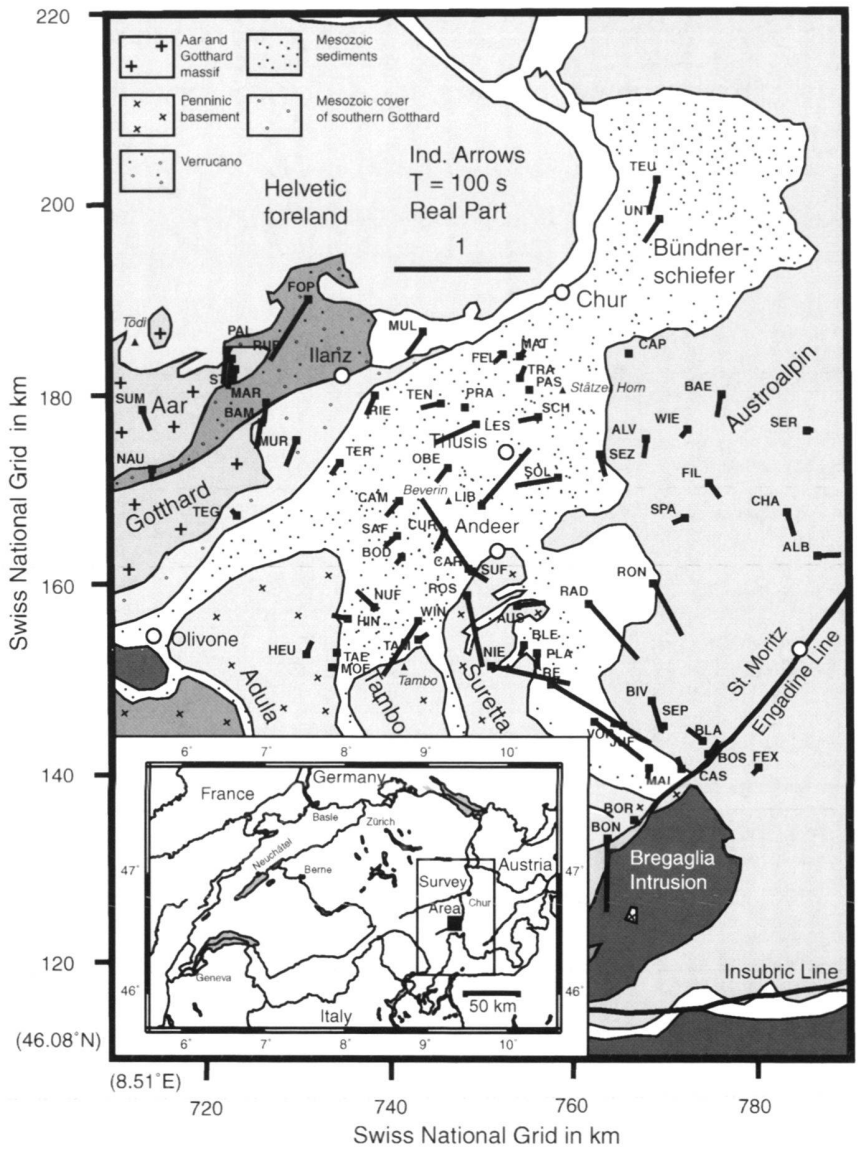

Fig. 1. Location of the investigation area (inlet) and real induction arrows in Graubünden for the 64 MT/GDS sites (filled squares) for the period T= 100 s. The lower left corner refers to coordinate: (λ= 8.51°E / ϕ= 46.08°N).

identify the Tschera nappe limits. These light weighted shallow depth high-resolution investigation techniques are ideally suited for the rugged alpine region of eastern Switzerland (Fig.1).

In contrast to the survey findings in the western Swiss Alps (Schnegg 1998), data collected in eastern Switzerland using the MT/GDS methods (Gurk 1999) revealed a change of direction in the real part of the induction arrows over the entire period range (T= 1-300 s). Induction arrows are a parameter of the induced magnetic field used to map lateral changes in the electrical conductivity distribution in the subsurface. Their change in direction in Graubünden coincides with the structural contact (SW-NE) between the Mesozoic Bündnerschiefer and the Penninic basement slices (Fig. 1). As the induction arrows point towards a region of lower electrical conductivity (Wiese 1962) a highly conductive zone was anticipated within this structural discontinuity. This major contact is therefore an important marker for understanding electromagnetic induction processes in the Central Alps. The notable change in the induction arrows direction between the two MT/GDS sites called CAR and SUF over the Tschera unit (Fig. 1) prompted further detailed investigations between these two locations using the above mentioned additional geophysical methods.

2 Survey area

2.1 Geological outline

The Tschera and Gelbhorn nappe (Fig. 2) are sub-units of the Schams nappe. The Schams nappe is the allochthonous part of the Mesozoic sedimentary cover of the imbricated Tambo/

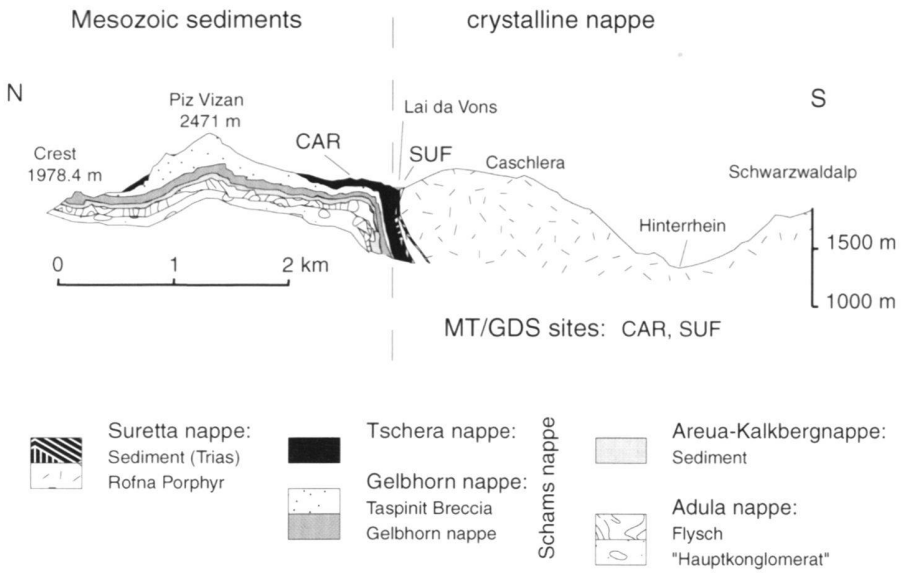

Fig. 2. Cross-section through the investigation area showing the steep sedimentary bands of the Schams unit in front of the hangingwall of the Suretta nappe. Redrawn from J. Neher in: Streiff et al. (1976).

Suretta basement slices. The structural contact with the Bündnerschiefer farther to the North and with the crystalline Suretta nappe to the South, is characterised by the presence of various sediments including Plattensandstein, anoxic black shales and various Triassic carbonates. The rocks form a compressed series of steep and deep reaching (detached) sedimentary bands divided by thrusts. The black shales exhibit a high organic carbon content (Schmid et al. 1990). The alteration of competent and incompetent layers creates an eroded, smoothly varying morphology without any remarkable outcrops. Consequently, detailed geological mapping of the units is difficult.

Figure 3 provides an overview of the survey area as well as the induction arrows for T = 100 s period of the two MT/GDS investigation sites CAR and SUF (Gurk 1999). Since the change of direction of the induction arrows in Graubünden is almost independent of the signal period (Gurk 1999), this change supports an initial hypothesis that a major lateral variation in conductivity might exist over these narrow sequences. As the induction arrows indicate a high conductivity zone, the following section deals with the different general mechanisms, which can explain the origin of such zones and the kind of conductive zone that might be likely in our survey area.

2.2 Origin of electric conductive zones

Structural discontinuities are promising candidates to create electrically conductive zones. Apart from high conductive structures caused by partial melts (Schmeling 1986; Shankland & Waff 1977), there are two other principal conductivity mechanisms producing low resistivity zones:

On one hand, elevated conductivities can result from electronically conducting ores such as interconnected graphite (ELEKTB-Gruppe 1994) or pyrite minerals. Alternatively, increased conductivities can also arise from an ionic current flow

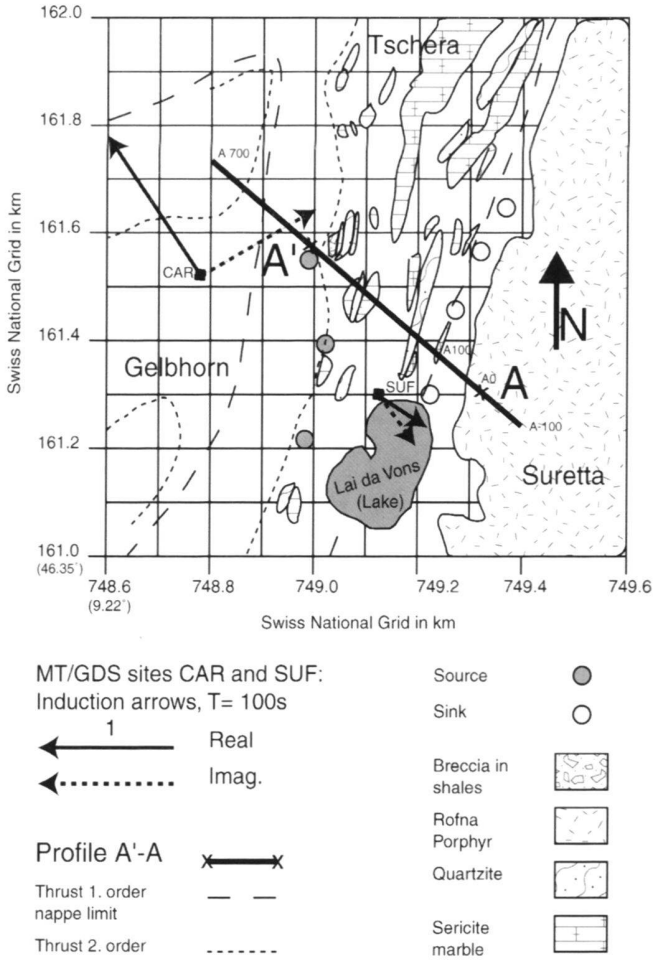

Fig. 3. Map of the investigation area. Redrawn from Streiff et al. (1971). The lower left corner refers to coordinate: (λ= 9.22°E / ϕ= 46.35°N).

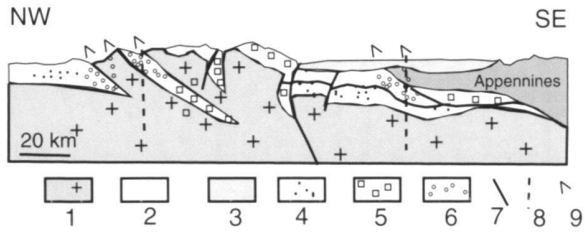

Fig. 4. Simplified section of the alpine arc showing a general model of fluid traps and fluid escape along deep reaching thrusts (Arthaud & Dazy 1989).

caused by fluids (Jödicke 1992). A general hydrological model for fluid transport and escape of brines in the Western Alps is summarised in Fig. 4 (Arthaud & Dazy 1989). The Arthaud & Dazy model reflects the tectonic setting of the stacked Penninic basement slices orientated either N-S or E-W. The expected enhanced electric conductivity along deep reaching thrusts in the studied contact zone could then be caused by brines migrating from the lower crust.

Figure 3 suggests that both conductivity mechanisms are feasible in the area of interest. Several springs and swallow holes are aligned along the major thrusts. However, the water in these springs has an electrical conductivity of up to 200 µS/cm (T= 26°C). These values contrast with conductivities in excess of 15000 µS/cm at T= 5.6°C (ca. 0.65 Ωm) measured in the Inn valley, 50 km to the East (Bissig 1997). The Scuol-Tarasp/Inn valley mineral springs isotopic CO_2 significance is typical for thermo-metamorphic reactions with carbonates (Wexsteen et al. 1988).

Beside the existence of springs and swallow holes in the survey area, metamorphic organic matter up to a coal rank of semi-graphite is present in Graubünden (Erdelbrock 1994; Mählmann 1995; Mählmann 1996). Weh et al. (1996) state, that in many cases, structural and metamorphic discontinuities coincide. Hence, due to the enhanced organic carbon content of the black shales in the Tschera unit, we expect, in analogy with the MT/GDS survey in the Valais Alps (Schnegg 1998) to find a graphite conductivity anomaly.

Apart from the non-linear induced polarisation method (Bigalke & Junge 1999), standard resistivity field surveys do not allow the difference between these two conductance mechanisms to be distinguished. However, SP-anomalies, for example, with magnitudes of several hundreds of millivolts provide strong evidence for the existence of electrically conducting ore minerals (Sato & Mooney 1960).

3 Geophysical survey methods and equipment

According to the initial hypothesis of a major lateral change in electrical conductivity in the survey area, as well as the previously mentioned different possibilities of its origin, different geophysical high resolution investigation methods for shallow depths were chosen to ascertain, which of the above mentioned hypotheses was most probable. The methods were:

- Self-potential,
- Magnetics and
- Radio Frequency-Electromagnetics.

The measurements were carried out along profile A (length: 800 m, orientation: 309° N, see Fig. 3) from the Suretta nappe to the Gelbhorn unit crossing the Tschera nappe nearly perpendicular to the fault boundaries.

The following sections explain the motivation for the application of these particular methods in this case history. Their main principles including particular sensitivities as well as data acquisition and equipment specifications are described briefly.

3.1 Self-potential

Ore mineralisation often produces a natural negative electrical potential along the earth's surface. SP-anomalies are nearly invariant in time and can have magnitudes of up to -1.8 V (Gay 1967). Thermoelectric and/or electrokinetic coupling processes

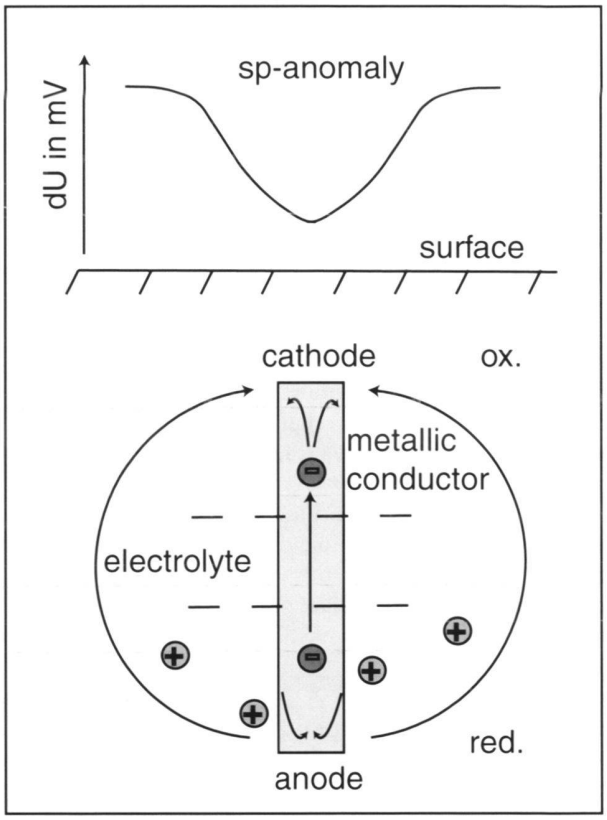

Fig. 5. A steeply inclined electronic conductor connects regions of different redox potential (ox: oxidation zone, red: reduction zone) and forms a "geobattery". The redox potential difference corresponds to an electron flow from the formation into the lower end of the electron conductor (anode). The electrons move to the upper end (cathode) and are transferred to the environment, (Sato & Mooney 1960).

can generate SP anomalies (Fittermann 1979), but they can also be produced by electrochemical processes similar to those in a galvanic cell. Geological structures showing such processes are called geobatteries (Sivenas & Beales 1982). The conceptual model of a self-potential anomaly caused by a geobattery is shown in Fig. 5. According to Sato & Mooney (1960) a steeply inclined metallic conductor (graphite, pyrite, ores, etc.) connects the oxidising country rock with the reducing environment at depth. Due to the chemical energy of the redox potential gradient, electrons flow within the conductor from its lower end – the anode of the battery – upwards to the cathode. The charge conservation is provided by a simultaneous flow of ions in the formation and the voltage drop at the surface can be measured as SP anomaly. Geobatteries may produce SP signals with magnitudes of several hundred millivolts and provide a strong indication for interconnected electronically conducting minerals (Bigalke & Grabner 1997; Stoll et al. 1995).

The self-potential measuring equipment consists of a pair of non-polarisable Cu-$CuSO_4$ electrodes arranged on a spade stick, and a voltmeter to measure the potential differences between the two electrodes. One electrode (the base) is kept fixed whereas the second electrode is used to sample the field every 20 m. On the anomalies the step is reduced to 1.0 m or less.

3.2 Magnetics

Due to the existence of magnetite in the Plattensandstein of the survey area, magnetics offered a promising means of obtaining information about the stratigraphy of the structural contact between the Bündnerschiefer and the crystalline Suretta nappe. The total magnetic field was measured using a Geometrics G 816 proton precession magnetometer. An initial 10 m sampling interval identified the main anomalies and the magnetic background. Over anomalies, the measuring interval is reduced to 1.0 or 0.2 m. All values were corrected for time variations using data of the Neuchâtel Geomagnetic Observatory.

3.3 Radio Frequency-Electromagnetic (RF-EM) method

The RF-EM method is an enhancement of the traditional VLF-EM (Very Low Frequency-Electromagnetic) method. It uses electromagnetic signals from permanently transmitting remote sources provided by terrestrial radio broadcasting antennas in the extended frequency range of 15–300 kHz.

The instrumentation used was developed at the Hydrogeology Centre of Neuchâtel (Stiefelhagen 1998; Turberg & Müller 1992; Turberg et al. 1994; Bosch & Müller 2001) with focus on the investigation of karst structures (Bosch & Gurk 2000) at shallow depths (10–100m). The instrument continuously measures the local horizontal and vertical magnetic field components with two orthogonal induction coils. For a chosen frequency, the device determines directly the "in-phase" and "out-of-phase" (also called "quadrature") components of the secondary to primary magnetic field's ratio, i.e. the real and imaginary part of the magnetic transfer function. Datalogging with 1 Hz or 4 Hz sampling rate can be chosen. Data obtained on a profile yield lateral resistivity contrasts in the subsurface that directly reflect geological features such as fractures, faults or facies/permeability variations. Due to the skin effect, profiling with various transmitter frequencies provides lateral resistivity contrast information for different penetration depths of the electromagnetic fields.

A handheld system was used for this survey. Compared to the imaginary parts, the real parts of the transfer function are much more affected by antenna deviations from the vertical caused by the continuously walking process. Consequently the real part data are of minor quality and are not subject of this paper. Some particular aspects of the method should be considered:

The RF-EM technique is a true 2D method and very sensitive for vertical structures. It obtains the magnetic transfer functions over a profile assuming E-polarisation. Therefore, the instrument actually yields the magnetic field components: $B_z/B_{y'}$, with y' normal to the strike of the structure. Vertical structures are indicated by the inflection points of the measured $B_z/B_{y'}$ curve (McNeill & Labson 1991). Due to transmitter availability and the nature of complicated geological structures, the precise E-polarisation case is not very likely. Consequently, a mixture of polarisation results in a distorted sounding curve. Additionally the dip of a buried conductor will deform the RF-EM response (McNeill & Labson 1991). These facts do severely impede the RF-EM interpretation. According to the main strike directions in the survey area and the chosen profile A-A' (Fig. 3), the 216 kHz transmitter fulfils quite well the case of E-polarisation. 20.3 kHz is unfortunately close to the H-polarisation case as listed in Table 1. 216 kHz was recorded with 4 Hz sampling rate and 20.3 kHz with 1 Hz. According to subsurface apparent resistivities of about 1000–3000 Ωm obtained in previous geoelectric mapping and soundings along the profile (not discussed in this paper), these frequencies provide estimated penetration depths δ shown in Table 1.

4. Observations Part I: Self-potential and Magnetics

A preliminary survey showed that all kinds of magnetic and SP anomalies are found with stable background values in the profile interval 0–320 m (A-A'). Hence, we restrict our presentation to this 320 m-long part of the profile. The results of

Tab. 1: Estimated *skin-depths* δ against *apparent resistivities* ρ_a of the subsoil and *signal frequency* f of the RF-EM technique (and direction of transmitter against North)

	ρ_a = 1000 Ωm	ρ_a = 3000 Ωm
f=216 kHz, 221° N	δ= 30 m	δ= 60 m
f=20.3 kHz, 144° N	δ= 110 m	δ= 192 m

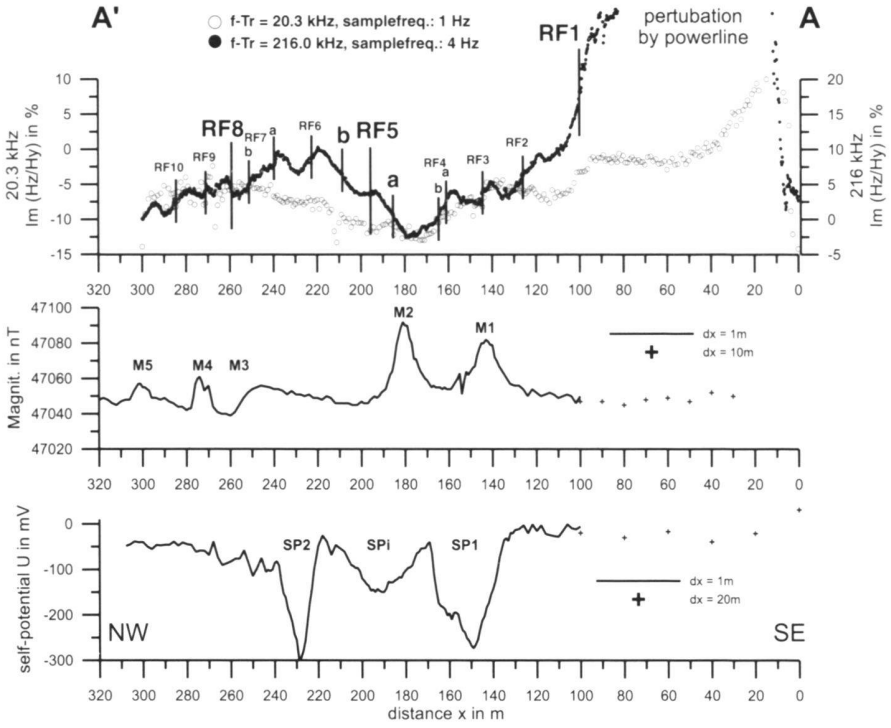

Fig. 6. RF-EM, total intensity of the magnetic field and self-potential measurements along the profile section A'-A.

the three applied profiling methods are presented in Fig. 6. The self-potential and the magnetic data show some sharp anomalies, whereas the RF-EM curve features a complex series of responses with superimposed signals. In the next sections, we confine ourselves on the description and interpretation of the self-potential and magnetic data. The modelling of the SP data then leads to a preliminary interpretation of the SP and magnetic anomalies series. Finally a description and interpretation of the RF-EM data are given and are used to confirm the results.

4.1 The series of SP and magnetic anomalies

The magnetic and SP values create an ordered series of anomalies:

Starting from SE the series begins with magnetic anomaly **M1** at 143 m, which is directly followed by a broad self-potential anomaly **SP1** with its minimum of about –270 mV at 149 m.

The series continues with the sharp magnetic anomaly **M2** at 181 m and the self-potential anomaly **SP2** measuring about –300 mV at 229 m. The intermediate self-potential anomaly **SPi** (190 m) between **SP1** and **SP2** reaches only -150 mV. Beyond 200 m the magnetic data show a smooth trend towards higher values which ends with a sudden step (**M3**) to lower magnitudes at 250–260 m. Two small anomalies **M4** and **M5** (274 m, 300 m) occur in the western part of the profile. Focussing on the magnitudes of the magnetic anomaly pairs (**M1/M2**), (**M4/M5**), we find that this series starts with a low amplitude anomaly (**M1**) followed by the high amplitude **M2** anomaly. The pair on the NW side of the profile shows the inverse pattern.

4.2 The shape of the self-potential anomalies

The dip of a buried conductor, ideally a dyke with infinite lateral extension, can be estimated from the shape of the anomaly. A vertical dyke, as shown in Fig. 5, produces a symmetric SP anomaly, whereas a dyke with a certain dip distorts the anomaly shape. Anomaly **SP2** is distorted such that the NW shoulder is lower than the SE shoulder. This behaviour corresponds to the model of a right dipping dyke (Telford et al. 1990). It is difficult to draw the same conclusion for **SP1**. This anomaly cannot be described by a simple dyke model. Nevertheless, a predominant right dipping feature seems to be present in the data for **SP1**. The **SPi** anomaly exhibits a small distortion effect implying a NW dipping structure.

4.3 The shape of the magnetic anomalies

Similar estimation about the dip of a buried dyke can be made for magnetic anomalies (Telford et al. 1990). But unfortunately, both magnetic anomaly pairs (**M1/M2**) and (**M4/M5**) are too close to each other. Therefore, no magnetic background values can be found between the anomalies and the analysis of their shape will be misleading. However, the sudden step (**M3**) to lower magnetic values, as mentioned above, is typical for a contact between two blocks of different susceptibilities (Telford et al. 1990).

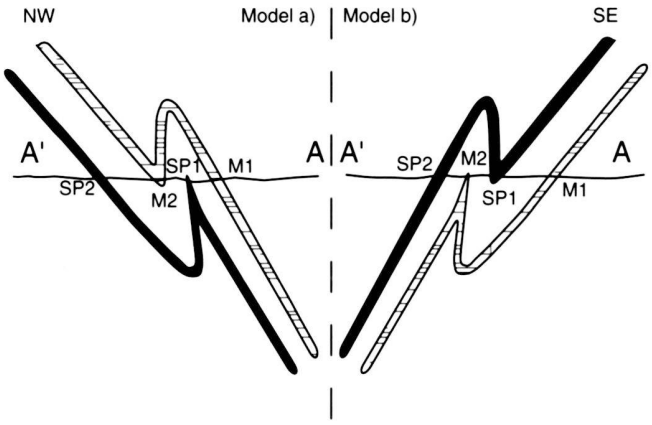

Fig. 7. Two equivalent explanations for the observed series of magnetic and self-potential anomalies **SP2 – M2 – SP1 – M1.**

5 Preliminary interpretation of the SP and magnetic anomalies series

The sequence of magnetic and SP anomalies:

SP2-M2-SP1-M1

may be interpreted in stratigraphical and tectonic terms. According to the geological map (Fig. 3, Streiff et al. (1971)) we can assume that both types of anomaly in this series are caused by the same lithology. Fig.7 shows that this series then can be interpreted as tight folds, which are dipping either (a) SE or (b) NW.

Model (b) is less probable since the analysis of the shape of anomaly **SP2** reflects a south dipping structure. However, the dip angle and the extension with depth of the strata remain uncertain. The SP data may be modelled to delineate the most realistic fold geometry (Fig. 8).

5.1 Self-Potential Model

The modelling has been performed at the University of Frankfurt/Main using the approach method of Bigalke & Grabner (1997) which includes an electrochemical model of the redox potential distribution. It was necessary to split the self-potential data into two branches and to limit the sample interval to 3.5 m. The intermediate anomaly **SPi** was excluded from the modelling. Each branch has been treated separately.

The most striking feature is the good match of both models. The first conductor, responsible for anomaly **SP2**, plunges southwards down to a depth of 40 m and with a dip of about 45°. If extrapolated, the conductor finds its continuation in the 80° northwards and 62° southwards dipping limbs of the anticline structure of the second conductor. Although we did not take the **SPi** anomaly into account, the model fits the field data sufficiently well. Generally, the model confirms our former analysis of the ordered anomaly series. Yet, the origin of the **SPi** anomaly is still unknown.

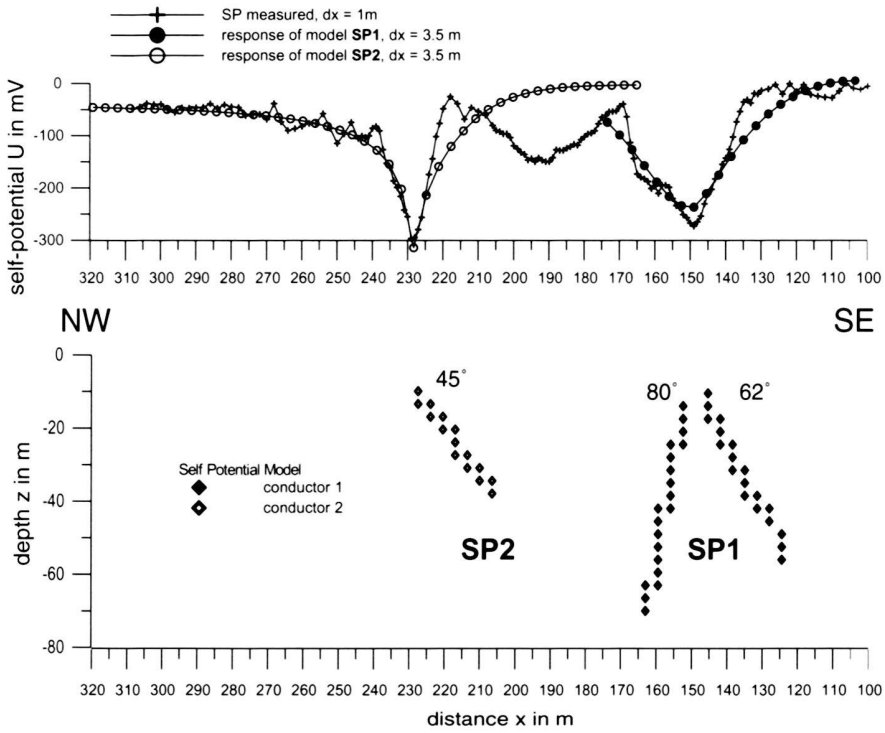

Fig. 8. Model of the self-potential data and its response.

6 Observations Part II and interpretation of RF-EM sounding curves

In this section the RF-EM data are described and interpreted in comparison with the results from SP and magnetic data.

The RF-EM curves of the imaginary part of the B_Z/B_Y ratio show superimposed anomalies (Fig. 6), which indicate lateral resistivity contrasts at the specific penetration depths. The 216 kHz curve shows more variations with higher amplitudes than the 20.3 kHz curve, which is of poorer quality. It is likely that the missing variations in the 20.3 kHz quadrature curve are a result of the H-polarisation case for this frequency. Therefore, we focus on the 216 kHz curve. An electric powerline crosses the profile at 0 m and influences the RF-EM measurements for 216 kHz up to ca. 80 m and up to ca. 40 m for 20.3 kHz. The different anomalies are named **RF1** to **RF10,** from SE to NW (Fig. 6).

The most striking resistivity contrasts are indicated by **RF1** (visible for both frequencies) at 100 m and by **RF5**. The latter is a superposition of two signals (**RF5a** at 185 m & **RF5b** at 209 m) which are far away enough from each other to be separated by the 216 kHz band. The centre of **RF5** lies at 90 m and is therefore at the same position as **SPi**, whereas it's eastern edge is at 180 m, the same position as **M2**. These two big RF-EM anomalies show amplitude variations of up to 15 % indicating strong geological discontinuity zones. The geological map in Figure 3 shows that anomaly **RF1** coincides with a 1st order thrust, the structural contact between the Rofna Porphyr and the Tschera nappe. The intensity of anomaly **RF5** supports the argument for a thrust producing **SPi**. Anomaly **RF2** at 134 m also has a remarkable change in amplitude of 7.5 %, but magnetic and SP data show only very small variations at this position. The series of the anomalies **RF6** (221 m) / **RF7a** (239 m) lies at the edges of **SP2**. These two RF-EM anomalies may therefore indicate the edges of a conductive dyke, which shows up as **SP2**. This situation is similar for the sequence **RF3** (144 m) / **RF4a** (161 m) / **RF4b** (165 m) compared with **SP1**. **RF3** coincides with **M1**, whereas **RF8** coincides with **M3** at 260 m confirming the conclusion of an almost vertical contact between two blocks drawn from the magnetic curve shape. **RF9** at 271 m coincides with **M4**. The RF-EM anomaly pattern confirms the anomalies from SP and magnetic data quite well, but cannot explain their origin as stand-alone information.

7 Geological survey and synoptic model along the profile

We investigated the anomalies along the profile A'-A by coring and rock sampling. The main findings are listed in Table 2. The magnetic and RF-EM anomalies (**M1/ RF3, M2**) and (**M4/ RF9, M5**) are generated by the (exposed) magnetite bearing Plattensandstein.

Black shale with a high graphite content corresponds to the **SP1** and **SP2** anomalies, whereas the **SPi** anomaly occurs where only strongly weathered gneiss was found. From this observation and from the findings of the previous section, we conclude that the **SPi** anomaly and the strong gradient in the 216 kHz RF-EM data (**RF5**) are caused by a thrust. It extends, dipping slightly to the NW, down to a maximum depth of 30-110 m. This conclusion leads to the synoptic model presented in Fig. 9: Compression of the isoclinal folds (see Fig. 9c) leads to a detachment along the most incompetent series (black shale) of the folded Tschera nappe. The projected effective direction of the magnetisation in the Plattensandstein onto the profile will then create the observed change in the amplitudes of the magnetic anomaly pairs (**M1/M2**) and (**M4/M5**).

Tab. 2. Type of geophysical anomaly, lithology after Streiff et al. (1971) and strike and dip values along the profile section A'-A.

x in m	Anomaly	Lithology
100	**RF1**	thrust (structural contact Tschera/Rofna porphyr)
143	**M1 / RF3**	exposed Plattensandstein ("Gault") with magnetite (285° N / 68°)
149	**SP1**	exposed graphitic blackshale (285° N/ 79°)
161	**RF4a**	
165	**RF4b**	
179		exposed sericite marble (302° N / 67°)
181	**M2**	Plattensandstein ("Gault") with magnetite
185	**RF5a**	
192	**SPi / RF5**	strongly weathered gneiss, dip to NW, thrust
209	**RF5b**	
221	**RF6**	
229	**SP2**	Graphitic blackshale (ca. 2 m overburden by strongly weathered gneiss)
239	**RF7a**	
250	**RF7b**	
260	**M3 / RF8**	thrust, contact between two units of different susceptibility
274	**M4 / RF9**	(123° N / 69°) Plattensandstein ("Gault")
284	**RF10**	
290	**M5**	(123° N / 78°) Plattensandstein ("Gault")

8 Conclusion

A case history for an integrated geophysical survey has been presented to separate magnetic and self-potential anomalies over a narrow sequence of detached sedimentary bands. The combination of self-potential, RF-EM and magnetic measurements provides a high-resolution technique to investigate structural contacts in the absence of reliable outcrops. The synoptic model explains the combined results of applied geophysical methods and geological in-situ information. The RF-EM method is the most rapid technique and detects resistivity contrasts with the highest lateral resolution, but does not identify their origin because of its sensitivity for resistivity contrasts caused by different mechanisms. The geophysical findings and the modelling of the SP data agree well with the geological analysis of the sequence. Moreover, the survey was able to confirm the known geology at this locality and could detect two additional thrust faults in the Tschera unit. The presence of interconnected graphite is confirmed by the SP method.

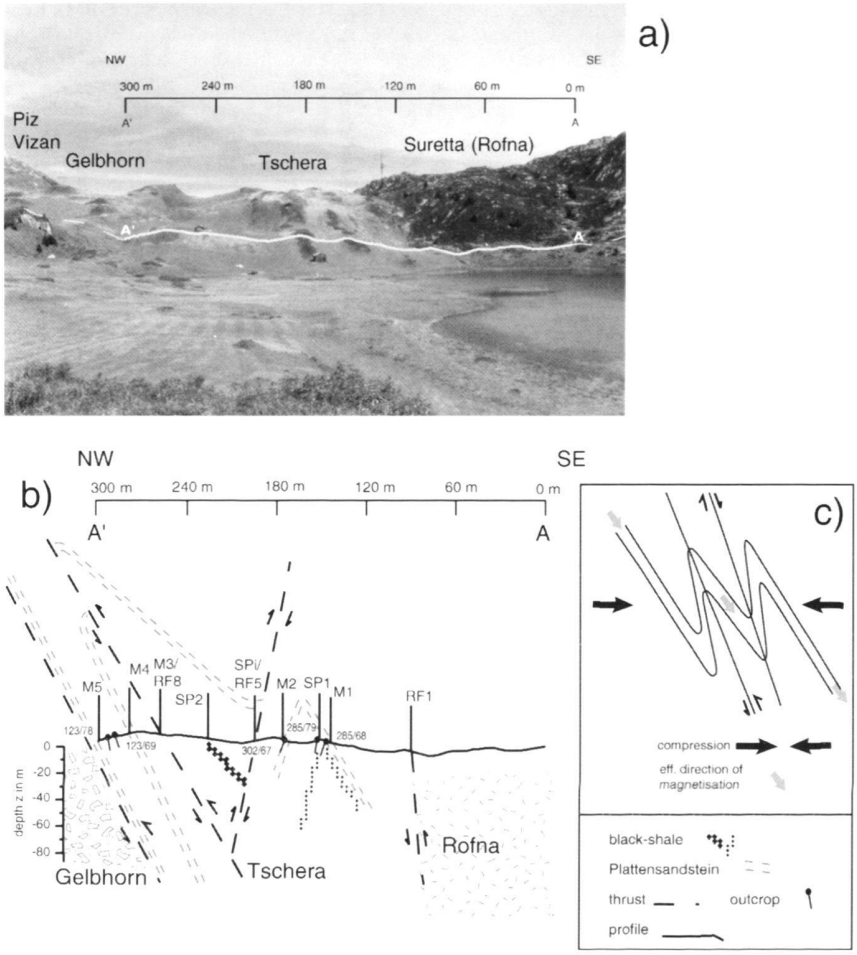

Fig. 9. (a) View parallel to the structural contact and (b & c) synoptic model of the fold geometry of the Tschera nappe along the profile section A'-A together with geophysical anomaly positions.

On a more regional scale, the electrical properties offered by the Tschera nappe are not sufficient to create a large conductive zone which could be responsible for the directional dualism of the GDS real induction arrows observed in Graubünden over long periods (T > 10 s). Consequently, the direction change of the real part of the induction arrows is more likely the result of a current channelling (Gurk 1999).

Acknowledgements

The Swiss National Foundation financially supported the research presented in this paper. The authors are very indebted to Mr Jaques Duperrex who built the electromagnetic equipment used in this study.

REFERENCES

ARTHAUD, F. & DAZY, J. 1989: Migration des saumures au front des chevauchements de l'arc alpin occidental. C. R. Acad. Sci. Paris. 309 (Sér. 2), 1425–1430.

BIGALKE, J. & GRABNER, E.W. 1997: The Geobattery Model: A contribution to large scale Electrochemistry. Electrochimica Acta 42 (23–24), 3443–3452.

BIGALKE, J. & JUNGE, A. 1999: Using evidence of non-linear induced polarization for detecting extended ore mineralisations. Geophys. J. int. 137, 516–520.

BISSIG, P. 1997: Hydrogeologische Untersuchung der CO2-reichen Mineralquellen von Scoul-Tarasp (GR, Schweiz). Diploma thesis, Centre de Hydrogéologie, Neuchâtel, Neuchâtel, 91 pp.

BOSCH, F.P. & GURK, M. 2000: Comparison of RF-EM, RMT and SP measurements on a karstic terrain in the Jura Mountains (Switzerland). Proceed. of the Kolloq. elektromagnet. Tiefenforsch., Altenberg/Bergisches Land, Germany, Mitt. Dtsch. geophys Ges. 18, 51–59.

BOSCH, F.P. & MÜLLER, I. 2001: Continuous gradient VLF measurements: A new possibility for high resolution mapping of karst structures. First Break 19 (6), 343–350.

ELEKTB-GRUPPE: BAHR, K., BIGALKE, J., EISEL, M., HAAK, V., HARMS, U., HIRSCHMANN, G., HUENGES, F., JÖDICKE, H., KOTNY, A., KÜCKE, J., NOVER, G., RAUEN, A., STOLL, J., WALTHER, J., WINTER, H. & ZULAUF, G. 1994: Untersuchungen zur elektrischen Leitfähigkeit in der Kontinentalen Tiefbohrung und ihrem Umfeld – was bringt sie uns Neues? Mitt. dtsch. geophys. Ges. 4, 2–40.

ERDELBROCK, K. 1994: Diagenese und schwache Metamorphose im Helvetikum der Ostschweiz (Inkohlung und Illit-"Kristallinität"). PhD thesis, Fakultät für Bergbau, Hüttenwesen und Geowissenschaften, Rheinisch-Westfälische Technische Hochschule Aachen, Aachen, 220 pp.

FITTERMANN, D.V. 1979: Calculation of self-potential anomalies near vertical contacts. Geophysics 44, 195–205.

GAY, S.P. 1967: A 1800 Millivolt Self-Potential Anomaly near Hualgayoc, Peru. Geophys. Prosp. 15, 236–245.

GURK, M. 1999: Magnetic Distortion of GDS Transfer Functions: An Example from the Penninic Alps of Eastern Switzerland Revealing a Crustal Conductor. Earth Planets Space 51, 1023–1034.

JÖDICKE, H. 1992: Water and graphite in the earth's crust – an approach to interpretation of conductivity models. Surv. in Geophys. 13, 381–407.

MÄHLMANN, R.F. 1995: Das Diagenese-Metamorphose-Muster von Vitrinitreflexion und Illit-"Kristallinität" in Mittelbünden und im Oberhalbstein Teil 1: Bezüge zur Stockwerkstektonik. Schweiz. mineral. petrogr. Mitt 75. 85–122.

MÄHLMANN, R.F. 1996: Das Diagenese-Metamorphose-Muster von Vitrinitreflexion und Illit-"Kristallinität" in Mittelbünden und im Oberhalbstein Teil 2: Korrelation kohlenpetrographischer und mineralogischer Parameter. Schweiz. mineral. petrogr. Mitt. 76, 23–46.

MCNEILL, J.D. & LABSON, V.F. 1991: Geological mapping using VLF radio fields. In: Electromagnetic Methods in Applied Geophysics Volume 2, Application, Parts A and B (Ed. by M.N. NABIGHIAN). Investigations in Geophysics, 3, Society of Exploration Geophysicists, Tulsa Oklahoma, Tulsa, 521–640.

SATO, M. & MOONEY, H.M. 1960: The Electrochemical Mechanism of Sulfide Self-Potentials. Geophysics XXV(1), 226–249.

SCHMELING, H. 1986: Numerical models on the influence of partial melt on elastic, anelastic and electrical properties of rocks. Part II, electrical conductivity. Phys. Earth Planet. Inter. 43, 123–135.

SCHMID, S.M., RÜCK, P. & SCHREURS, G. 1990: The significance of the Schams nappes for the reconstruction of the paleotectonic and orogenic evolution of the Penninic zone along the NFP-20 East traverse (Grisons, eastern Switzerland). Mém. Soc. géol. France 156, 263–287.

SCHNEGG, P.-A. 1998: The magnetotelluric survey of the Penninic Alps of Valais. Matériaux pour la Géologie de la Suisse – Geophysique 32, Swiss Geophysical Commission, Bern, 76 pp.

SHANKLAND, T.J. & WAFF, H.S. 1977: Partial melting and conductivity anomalies in the upper mantle. J. geophys. Res. 82, 5409–5417.

SIVENAS, P. & BEALES, F.W. 1982: Natural geobatteries associated with sulphide ore deposits, I. Theoretical Studies. J. geochem. Explor. 17, 123–144.

STIEFELHAGEN, W. 1998: Radio Frequency Electromagnetics (RF-EM): Kontinuierlich messendes Breitband-VLF, erweitert auf hydrogeologische Problemstellungen. PhD thesis, Centre of Hydrogeology, University of Neuchâtel, Neuchâtel, Switzerland, 243 pp.

STOLL, J., BIGALKE, J. & GRABNER, E.W. 1995: Electrochemical Modelling of Self-Potential Anomalies. Surv. in Geophys. 16, 107–120.

STREIFF, V., JÄCKLI, H. & NEHER, J. 1971: Geologischer Atlas der Schweiz, Blatt: 1235 Andeer. Kommissionsverlag: Kümmerly & Frey AG Geographischer Verlag Bern, Bern, 1:25 000.

STREIFF, V., JÄCKLI, H. & NEHER, J. 1976: Erläuterungen zu Blatt: 1235 Andeer, Kommissionsverlag: Kümmerly & Frey AG. Geographischer Verlag Bern, Bern, 106 pp.

TELFORD, W.M., GELDART, L.P. & SHERIFF, R.E. 1990: Applied Geophysics, Cambridge University Press, Cambridge, 770 pp.

TURBERG, P. & MÜLLER, I. 1992: La méthode inductive VLF-EM pour la prospection en continu de milieu fissuré. Proceed. of the Cinquième Coll. d'Hydrol. en Pays calcaire, Neuchâtel, 16–18.10, Ann. Sci Univ. Besançon Géologie, 207–214.

TURBERG, P., MÜLLER, I. & FLURY, B. 1994: Hydrogeological investigation of porous environments by radio magnetotelluric-resistivity (RMT-R 12–240 kHz). J. appl. Geophys. 31, 133–143.

WEH, M., MÄHLMANN, R.F. & FROITZHEIM, N. 1996: Strukturelle und metamorphe Diskontinuitäten im Penninikum am Westrand der Ostalpen. Proceed. Tektonik und Strukturgeologisches Kolloqium.

WEXSTEEN, P., JAFFÉ, F.C. & MAZOR, E. 1988: Geochemistry of cold CO2 –rich springs of the Scuol-Tarasp region, Lower Engadine, Swiss Alps. J. Hydrol. 104, 77–92.

WIESE, H. 1962: Geomagnetische Tiefentellurik Teil II: Die Streichrichtung der Untergrundsstrukturen des elektrischen Widerstandes, erschlossen aus geomagnetischen Variationen. Geofis. pura Appl. 52, 83–102.

Manuscript received November 24, 1999
Revision accepted July 25, 2001